International Journal of Engineering and Technology Innovation, vol. 16, no. 2, 2026, pp. 266-283

Machining Quality Prediction in Stainless Steel Side Milling Using Neural Networks

Ming-Hsu Tsai[1,*], Jeng-Nan Lee[1], Teng-Hui Chen[1], Tai-Lin Hsu[2], Dong-Ke Huang[2]

[1]Department of Mechanical Engineering, Cheng Shiu University, Kaohsiung, Taiwan, ROC

[2]Institute of Mechatronics Engineering, Cheng Shiu University, Kaohsiung, Taiwan, ROC

Received 28 February 2026; received in revised form 09 April 2026; accepted 20 April 2026

DOI: https://doi.org/10.46604/ijeti.2026.16217

Abstract

This study proposes a novel neural network-based framework to predict machining quality during the side milling of SUS304 stainless steel. As a holistic deep neural network (DNN) framework bridging real-time sensory cutting forces to dual quality metrics—dimensional accuracy and surface roughness—this research addresses a critical gap in SUS304 intelligent machining. A sensory tool holder acquires cutting force signals while an automated in-process system measures machining outcomes. DNN and convolutional neural network (CNN) models are trained using frequency-domain features. Results indicate that the DNN achieves superior robustness, with an average root mean square error (RMSE) of 0.0194 mm for dimensional accuracy and 0.3950 μm for surface roughness. Statistical validation via the mann-whitney u test ($p < 0.005$) confirms that the DNN more effectively captures global nonlinear relationships within spectral features. This research validates a reliable, high-precision framework for in-process quality prediction, supporting adaptive control in difficult-to-machine materials.

Keywords: SUS304 stainless steel, in-process quality prediction, neural networks, sensory tool holder

1. Introduction

The advent of Industry 4.0 has propelled manufacturing toward greater digitalization and intelligent automation, driven by the goals of enhancing operational efficiency, production flexibility, and long-term sustainability. At the heart of this transition lies the integration of key enabling technologies such as the internet of things (IoT), big data analytics, and machine learning—the latter offering powerful capabilities in pattern recognition and adaptive optimization within smart manufacturing and quality control systems. Conventional offline inspection is often time-intensive and prone to human error. To address this, the implementation of in-process measurement systems enables proactive defect detection.

By monitoring surface roughness as a tool wear indicator, these systems also support the development of comprehensive manufacturing databases. A persistent research gap remains concerning the seamless integration of artificial neural networks (ANNs) with sensory tool holders—devices equipped with embedded sensors capable of wirelessly transmit real-time cutting force data.

This work delineates that gap by proposing a novel ANN-based framework to predict key workpiece quality metrics, including dimensional accuracy and surface roughness, directly from sensory tool holder data. The overarching objective is to synchronize real-time data analytics with automated process control, advancing dimensional precision, boosting production efficiency, and ensuring consistent product quality in intelligent machining environments.

*Corresponding author. E-mail address: k0635@gcloud.csu.edu.tw

Stainless steel is widely utilized in industrial applications due to its high strength, thermal resistance, and corrosion resistance. However, its low thermal conductivity and significant work-hardening characteristics make it a challenging material to machine. These inherent properties often result in significant cutting forces and rapid tool wear during the machining process. Prior research by Chien and Chou [1] established a predictive model for the machinability of 304 stainless steel, examining the complex interactions between cutting speed, feed rate, and depth of cut. In advanced manufacturing, Tsai et al. [2] used 5-axis machining for SUS304 side milling and noted that the high toughness of the material leads to plastic deformation and negative stock deviation. Recent studies by Wang et al. [3] further highlight that the adhesiveness and ductility of 304 stainless steel facilitate the formation of a Built-Up Edge (BUE), which accelerates tool wear and significantly increases cutting forces. While these studies provide foundational knowledge on SUS304, they often rely on static parameters and lack real-time adaptability.

Surface roughness and dimensional accuracy serve as primary indicators of workpiece quality, which are often subject to the nonlinear influences of feed rate, depth of cut, and system vibrations. To acquire high-fidelity data proximal to the cutting zone, intelligent tooling systems have been developed to measure cutting forces, vibrations, and temperatures. Schuster et al. [4] developed a multi-sensory tool holder designed for process force monitoring and chatter detection. Complementary to these advancements, Souflas et al. [5] showcased an indexable milling head with integrated force and temperature sensing capabilities, providing a direct interface with the cutting phenomena.

Ojha et al. [6] explored optimization techniques for surface roughness prediction in turning operations. To address the need for real-time monitoring, Huang [7] proposed an intelligent neuro-fuzzy model for in-process surface roughness assessment. Lu et al. [8] developed an indirect monitoring method using a wireless sensing tool holder and the deep forest algorithm. Regarding dimensional errors in thin-walled milling, Chen et al. [9] implemented a sensing tool holder to establish path compensation models for elastic deformation. Further investigations by Nowakowski et al. [10] and Tsai et al. [11] extended this research scope to aluminum and titanium alloys, highlighting the critical influence of milling conditions and sensor-based feedback on the prediction of machining performance. These studies identified the feed rate as a key determinant of milling quality.

Tool wear directly degrades surface quality and escalates manufacturing costs. The real-time monitoring of tool wear is critical for maintaining machining quality and mitigating the costs associated with unplanned downtime. Early implementations combined ANN with genetic algorithms (GA) to predict tool life and optimize metal removal rates. Recent research has pivoted toward multi-sensor information fusion and deep learning architectures.

Krishnakumar et al. [12] utilized vibration signals and ANN to classify tool conditions in high-speed machining. Huang et al. [13] introduced a deep convolutional neural network (DCNN) based on multi-domain feature fusion for continuous wear prediction. Diverse architectures have been proposed, including milling force coefficient-based monitoring [14], convolutional bidirectional long short-term memory (LSTM) networks [15], and comparative studies of convolutional neural network (CNN), LSTM, and gated recurrent unit (GRU) frameworks [16]. In 2024, research further refined feature extraction using 1-D CNN and temporal convolutional networks (TCN) to handle long-term dependencies [17-18].

Souflas et al. [5] integrated both cutting force and temperature data from instrumented milling heads for the effective identification of initial, steady, and accelerated wear phases. Despite advancements in sensory tools and artificial intelligence (AI), most research treats signal features as local transients, overlooking the global spectral shifts characteristic of stable SUS304 milling.

The integration of mechanical cutting force models with AI algorithms allows for high-precision modeling and simulation of dynamic machining phenomena. Zagórski et al. [19] utilized ANNs to model cutting force components in milling operations.

Furthermore, Gao et al. [20] established a generic cutting force model that comprehensively considers tool edge radius, flank wear, and tool runout, particularly for micro-end milling applications. Integrating force models with AI shows promise; however, a holistic framework that bridges high-frequency sensory data with dual-quality metrics remains unexplored. While CNNs have gained traction for their ability to extract localized temporal features—such as impact impulses from tool chipping [11, 15]—their efficacy is often limited when processing frequency-domain signals derived from stable cutting phases. In SUS304 milling, phenomena like work-hardening and progressive flank wear do not typically manifest as isolated spectral peaks, but rather as a global redistribution of energy across the frequency spectrum.

A significant research gap exists in understanding how different neural architectures interpret these global versus local signal characteristics. This study tackles this gap by proposing a holistic framework that leverages deep neural networks (DNNs). Unlike CNNs, which prioritize spatial locality through kernel filters, DNNs utilize fully connected layers to capture global nonlinear correlations across the entire spectral domain. This research aims to bridge real-time sensory data with dual quality metrics, providing both a high-precision prediction tool and physical insight into model-signal alignment.

This study aims to develop an intelligent monitoring system that integrates data analytics with automated control to optimize the machining process of SUS304 stainless steel. The core objective is to utilize a sensory tool holder to acquire real-time cutting force signals, which serve as critical input features for DNN and CNN. By correlating physical signals with dual-target workpiece quality—dimensional accuracy (measured in-process) and surface roughness (measured offline)—this research seeks to stabilize product quality and lower manufacturing costs. The rest of this paper is organized as follows: Section 2 describes the experimental setup and the formulation of the neural network architectures; Section 3 presents the validation results and discusses the comparative performance of the models, including a parametric analysis. Finally, Section 4 summarizes the main conclusions and future research directions.

2. Materials and Methods

This section delineates the systematic approach developed to investigate the correlation between cutting forces and machining quality. The experimental methodology integrates high-fidelity data acquisition with precise workpiece metrology to establish a reliable dataset for neural network training. By synchronizing real-time force monitoring with automated in-process measurements, the framework captures the complex dynamics of the SUS304 milling process.

2.1. Experimental material and equipment

This study utilizes a Tongtai CT-350 5-axis machining center to conduct SUS304 side milling experiments. A closed-loop data monitoring framework is constructed using a high-precision sensory tool holder for real-time cutting force acquisition and an automated measurement system for quality verification. This experimental setup enables the synchronized collection of physical machining signals and corresponding workpiece outcomes. To ensure data integrity and system reliability, the following instruments are integrated into the manufacturing environment:

(1) Experimental materials: SUS304 stainless steel: SUS304 is a predominant material in medical devices, chemical engineering, construction, and aerospace sectors due to its exceptional corrosion resistance, high strength, and excellent ductility. Despite these advantages, its high toughness and low thermal conductivity make it a difficult-to-machine material.

(2) Sensory tool holder and cutting tool: (i) pro-micron sensory tool holder: this device features internal sensors for 360° signal acquisition. It captures real-time axial force (tension), torque, and bending moments (X-Z, Y-Z) at a sampling frequency of 2500 Hz via wireless transmission. (ii) cutting tool: a Ø 10 mm tungsten carbide end mill is used for side milling of SUS304.

(3) Measurement systems: (i) renishaw OMP400 In-process Measurement: automatically triggered via the machining program, this system is used to measure workpiece dimensions directly on the machine with a precision of 0.001 mm. This allows for immediate compensation of errors caused by tool wear or machine thermal deformation. (ii) opt-scope white light interferometer: a 3-D white light interference microscope provides non-contact measurement of Sa, Sz, Ra, and Rz, offering higher fidelity than traditional contact-type probes.

2.2. Artificial neural networks (ANN)

Drawing inspiration from biological nervous systems, ANNs are computational models comprising interconnected nodes, or neurons. In this study, DNNs and CNNs are employed to model and analyze the captured sensor signals. To elucidate the distinctions in their architectural frameworks and data processing capabilities, the CNNs are methodologically categorized into 1-D and 2-D models for comparative analysis.

(1) DNN in machining prediction: ANNs simulate biological neural structures to model complex, non-linear functions through weight optimization and activation functions. When configured with multiple hidden layers, these evolve into DNNs. In the context of machining, DNNs utilize a fully connected architecture where each neuron is connected to every unit in the preceding layer. While DNNs effectively process static scalar data, such as average cutting forces or discrete machining parameters, they inherently lack the ability to perceive spatial or temporal correlations. Consequently, feeding raw high-frequency signals directly into a DNN often leads to parameter explosion and convergence difficulties.

(2) Comparative analysis of CNN architectures: 1-D vs. 2-D CNN: CNNs mitigate the limitations of DNNs through local perception and weight sharing, significantly reducing the total number of parameters. When processing time-series cutting signals, 1-D and 2-D convolutions offer distinct advantages, as summarized in Table 1. It should be noted that the terms "1-D" and "2-D" in this study refer to the dimensionality of the input data after preprocessing, not to the physical spatial dimensions of the cutting forces. Physically, the sensory tool holder provides three-dimensional force-related signals, but due to the rotational symmetry of side milling, the XZ bending moment alone captures the essential information, as elaborated in Section 2.4.1.

Table 1 Comparison Table of 1-D and 2-D CNNs

Architecture	Data input format	Feature extraction logic	Advantages in this study
1-D CNN	Frequency-domain spectral vector (1-D Array)	1-D kernel slides along the frequency axis	Excels at capturing global spectral patterns and gradual energy shifts; well-suited for FFT-based features.
2-D CNN	Reshaped 2-D matrix (2-D Matrix)	2-D kernel slides across both dimensions of the reshaped matrix	Allows experimentation with 2-D convolution, but lacks physical meaning due to disrupted frequency adjacency.

For the 1-D CNN, the input is a 1-D spectral vector (magnitude vs. frequency) obtained by applying fast the fourier transform (FFT) to the segmented bending moment signal. The 1-D convolution kernel slides along the frequency axis, making it well-suited for capturing global spectral patterns and gradual energy shifts. For the 2-D CNN, the same 1-D spectral vector is reshaped into a 2-D matrix (e.g., 25×20 or 50×10). This transformation allows the use of standard 2-D convolution and pooling operations, which can improve computational efficiency for matrix inputs. However, such reshaping does not preserve the natural adjacency among frequency bins and therefore fails to capture physically meaningful correlations.

2.3. Experimental procedure and machining parameters

This study utilizes SUS304 stainless steel with workpiece dimensions of $75 \times 75 \times 60$ mm. The experimental procedure is executed in the following sequential stages:

(1) Preparation: pre-machining the SUS304 raw stock to the dimensions required for the experimental design.

(2) Parameter planning: defining the cutting conditions and process variables.

(3) Numerical control (NC) programming: developing the machining and in-process measurement programs using CAM and specialized metrology software.

(4) Machining and data acquisition: executing the cutting process while simultaneously capturing real-time cutting force signals and dimensional accuracy data.

(5) Offline metrology: measuring tool wear and surface roughness using precision instruments.

(6) Data integration: consolidating the acquired datasets to facilitate pre-processing for neural network training.

A total of 1,326 experimental trials are conducted using new Ø 10 mm tungsten carbide end mills. For each trial, cutting force signals from the sensory tool holder and dimensional measurement results are collected. To monitor the progression of machining quality, tool wear inspection and surface roughness measurements are performed every 26 trials (corresponding to one completed workpiece), resulting in 51 sets of detailed quality data.

2.3.1. Machining strategy and cutting parameters

Side milling is selected as the primary machining strategy. To mitigate volumetric errors caused by thin-wall elastic deformation, a 10 mm side-wall buffer is maintained throughout the experiments to ensure structural rigidity. The machining paths are generated using Mastercam 2021. This schematic diagram of the cutting path and direction is shown in Fig. 1.

The specific cutting parameters are summarized in Table 2. The experiments utilized a constant radial depth of cut (Ae) of 2.5 mm and an axial depth of cut (Ap) of 10 mm. Furthermore, a cutting speed of 70 m/min and a feed per tooth of 0.06 mm/tooth are adopted.

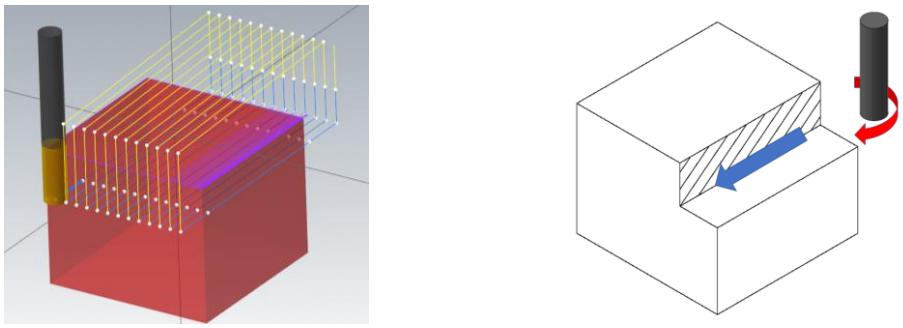

(a) Machining path planning (b) Schematic diagram of cutting direction

Fig. 1 Tool path planning and the schematic diagram of cutting direction

Table 2 Machining parameters

Cutting speed Vc (m/min)	Feed per tooth Fz (mm/tooth)	Rotational speed S (rpm)	Feed rate F (mm/min)	Axial depth of cut Ap (mm)	Radial depth of cut Ae (mm)
70	0.06	2228	500	10	2.5

2.3.2. In-process measurement system

The in-process measurement is implemented using Productivity+ Active Editor Pro. This system facilitates automated dimensional inspection by triggering a probe cycle immediately after machining. The integration of the Renishaw OMP400 probe within the NC program allows for real-time acquisition of workpiece dimensions without removing the part from the machine, thereby achieving a fully automated data collection loop. The measurement path planning and verification schematic is illustrated in Fig. 2.

(a) In-process measurement path planning (b) Measurement virtual verification

Fig. 2 Virtual verification of measurement based on in-process path planning

2.3.3. Surface roughness characterization

Surface roughness is analyzed using a 3D white-light interference microscope. Given the 1,326 total trials, measurements are taken at 26 trial intervals. For each sampled surface, data are captured at three distinct measurement points to ensure statistical reliability. These three values are subsequently averaged to determine the final roughness value for that interval. Data processing was performed via Surfcom Map Opt 8.0 software to extract four profile parameters: Sa, Sz, Ra, and Rz. This comprehensive characterization provides the necessary ground-truth labels for evaluating the ANN's prediction capabilities.

2.4. Signal acquisition and data pre-processing

Before model training, raw cutting force signals must undergo a series of preprocessing steps to extract meaningful features. The acquired time-domain signals contain high-frequency noise and non-stationary components inherent to the milling process. Therefore, a systematic preprocessing pipeline is essential to convert raw sensor outputs into a compact, informative representation suitable for neural network input. This pipeline consists of three main stages: signal segmentation, fourier transform-based frequency-domain conversion, and feature vector construction.

2.4.1. Cutting signal acquisition

The sensory tool holder captures six categories of data during the machining process: axial force (tension), torque (torsion), bending moment in the XZ and YZ planes, time, and temperature, as schematically illustrated in Fig. 3. Due to tool rotation, the XZ and YZ bending moments are phase-shifted but carry equivalent amplitude information. Therefore, the XZ bending moment is selected as the representative input feature for neural network training. Comprehensive cutting information and real-time waveforms are visualized and managed using the SPIKE Tool Analyser 2016 EN software.

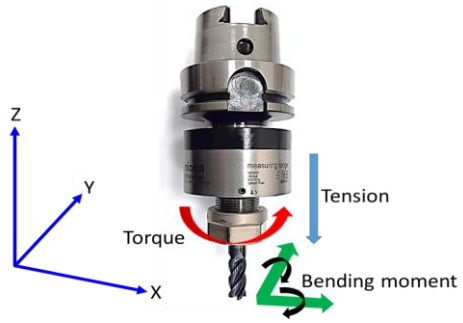

Fig. 3 Schematic of the pro-micron sensory tool holder and its measured physical quantities

2.4.2. Signal pre-processing and feature extraction

The effective cutting time for each experimental trial is approximately 9 seconds. With a sampling frequency of 2500 Hz, each trial generates approximately 22,500 data points. To facilitate neural network training, the following pre-processing steps are implemented:

(1) Window selection: a continuous segment of 1,000 sampling points is randomly selected from the stable cutting phase of each trial.

(2) FFT: these segments are transformed from the time domain into the frequency domain using FFT. In this study, the bending moment XZ is designated as the primary training feature due to its sensitivity to the tool-workpiece interaction.

For a uniformly sampled discrete-time signal $x[n]$ of length $N = 1000$ with sampling interval $\Delta t = 1/2500$ s, the standard discrete fourier transform (DFT) is defined as:

$$X[k] = \sum_{i=0}^{n-1} x[n] e^{-j2\pi kn/N},\ k = 0,1,...N-1 \tag{1}$$

where $X[k]$ represents the complex amplitude at frequency $f_k = k/(N\Delta t)$. In practical machining measurements, wireless transmission may occasionally introduce non-uniform sampling intervals due to packet loss or interference. To maintain accuracy under such conditions, a non-uniform DFT formulation is adopted:

$$X(\omega_k) = \sum_{i=0}^{N-1} x(t_i) e^{-j\omega_k t_i} \Delta t_i,\ \Delta t_i = t_{i+1} - t_i \tag{2}$$

This expression can be interpreted as a riemann-sum approximation of the continuous fourier transform. When the sampling instants t_i are equally spaced, it reduces to the standard DFT and can be computed via FFT. This transformation allows the raw time-domain cutting signals to be converted into high-dimensional spectral features, enabling the neural network to identify critical frequency components associated with machining stability.

After applying the fourier transform, only the first half of the spectrum (indices $k = 0$ to $N/2 - 1 = 499$) is retained. This is justified by:

(1) Nyquist criterion: the maximum resolvable frequency is $f_{\text{Nyq}} = 1/(2\Delta t) = 1250$ Hz, well above the dominant cutting force harmonics.

(2) Symmetry property: for real-valued signals, $X[k] = X^*[N-k]$; therefore, the second half provides no additional information.

(3) Dimensionality reduction: keeping only 500 frequency bins reduces the input size while preserving essential spectral features.

Finally, the resulting 500-point frequency-domain vectors are used as input features.

2.4.3. Training data configuration

Prior to neural network training, the processed data are structured into a specific input-output format suitable for supervised learning. The dataset for each trial is configured as follows:

(1) Input features: the first 500 frequency-domain data points derived from the FFT analysis serve as the feature vector.

(2) Target labels: the 501st data point is assigned as the target value. Two independent models are trained for distinct objectives: (i) dimensional error: derived from the in-process measurement system. (ii) surface roughness (Ra): derived from the 3D white light interference microscope.

By decoupling the training process for these two targets, the neural networks (DNN and CNN) can independently optimize the weight configurations for predicting macro-scale dimensional accuracy and micro-scale surface quality.

2.5. Program training architecture

To establish a reliable predictive model, a systematic training architecture is essential. This section outlines the configuration of the neural network training process, including dataset partitioning, model structures, and hyperparameter settings. Three types of networks are trained and compared under identical experimental conditions. The following subsections describe the data classification strategy and the specific architectural parameters for each model.

2.5.1. Dataset classification and training strategy

The experimental data are categorized based on the dual prediction targets: dimensional accuracy and surface roughness. For dimensional accuracy, 100 trials are randomly selected from the 1,326 total machining datasets. These are divided into a training set of 90 samples and a validation set of 10 samples. For surface roughness, all 51 available datasets are utilized, partitioned into 45 samples for training and 6 samples for validation. This classification strategy is summarized in Table 3.

Table 3 Classification of neural network training data

	Training set	Validation set	Target set
Training data	90	10	Dimensional accuracy
	45	6	Surface roughness

The training involves three neural network architectures: DNN, 1-D CNN, and 2-D CNN. The training/validation split ratios differ between the two prediction tasks due to the available sample sizes. For dimensional accuracy, 100 trials are randomly selected from the 1,326 total experiments, providing sufficient data to allocate 90 samples for training and 10 for validation (a 90/10 split). For surface roughness, only 51 datasets are available (one measurement per workpiece), which naturally limits the validation set size. A 45/6 split (approximately 88/12) is chosen to retain as many training samples as possible while keeping a meaningful validation set. To mitigate the risk of overfitting, given the smaller dataset for roughness prediction, loss curves are monitored to ensure convergence without divergence.

2.5.2. DNN configuration

The DNN models achieve convergence by optimizing the computational functions through various hidden layer depths (ranging from 3 to 5 layers), as illustrated in Fig. 4. Ten parameter groups (I to X) are evaluated, maintaining a constant learning rate (LR) of 0.00075, a batch size of 10, and 2,000 epochs. The specific neuron configurations for each layer are detailed in Table 4.

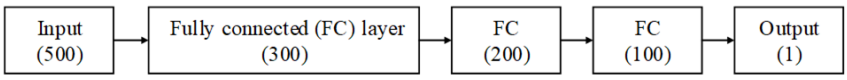

Fig. 4 Architecture of the DNN model used in this study

Table 4 Parameter settings of DNN

Model	I	II	III	IV	V	VI	VII	VIII	IX	X
First layer	300	400	350	400	300	250	350	400	250	400
Second layer	200	150	450	200	150	400	250	300	450	150
Third layer	100	50	125	300	250	150	150	200	200	300
Fourth layer	–	–	–	150	100	50	75	100	300	100
Fifth layer	–	–	–	–	–	–	–	50	100	75

2.5.3. 1-D CNN configuration

The 1-D CNN architecture is designed to process time-series input sequences of size 500, as shown in Fig. 5. The network parameters are tuned across ten experimental groups to reach convergence10. Key variables include kernel sizes ranging from 2 to 10, output channels between 2 and 20, and varying strides. Similar to the DNN, these models are trained for 2,000 epochs

with a batch size of 10. The learning rate is adjusted between 0.0005 and 0.001 to identify the optimal configuration. Other parameters are detailed in Table 5.

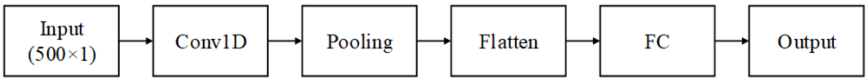

Fig. 5 Architecture of 1-D CNN for frequency-domain signal processing

Table 5 Parameter settings of 1-D CNN

Model	I	II	III	IV	V	VI	VII	VIII	IX	X
Convolution layer										
Input size	500	500	500	500	500	500	500	500	500	500
In channels	1	1	1	1	1	1	1	1	1	1
Out channels	2	2	2	2	2	2	2	4	8	20
Kernel size	2	4	6	6	6	6	6	10	10	10
Stride	1	2	4	4	4	4	4	4	4	4
Padding	1	1	1	1	1	1	1	1	1	1
Pooling layer										
Kernel size	2	2	2	2	2	3	5	8	8	10
Stride	1	1	1	1	1	2	4	4	4	2
Global hyperparameters										
Learning rate	0.001	0.001	0.001	0.0005	0.00075	0.00075	0.00075	0.00075	0.00075	0.00075

2.5.4. 2-D CNN configuration

For the 2-D CNN training, the 1-D input data is reshaped into two matrix dimensions: 25 × 20 and 50 × 10. This spatial restructuring allows the network to apply 2-D convolution and pooling kernels, as depicted in Fig. 6. Ten parameter sets are tested by adjusting the output channels and kernel sizes, which range from 1 to 4, to optimize model performance. Similar to the other models, 2,000 epochs and a batch size of 10 are employed across all configurations. The specific architectural details are detailed in Table 6.

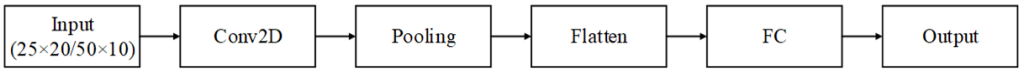

Fig. 6 Architecture of 2-D CNN reshaped spectral inputs

Table 6 Parameter settings of 2-D CNN

Model	I	II	III	IV	V	VI	VII	VIII	IX	X
Convolution layer										
Input size	25×20	25×20	25×20	25×20	25×20	50×10	50×10	50×10	50×10	50×10
In channels	1	1	1	1	1	1	1	1	1	1
Out channels	2	4	6	1	1	2	4	6	1	1
Kernel size	2	3	4	1	4	2	3	4	1	4
Stride	1	1	1	1	1	1	1	1	1	1
Padding	1	0	2	2	0	1	0	2	2	0
Pooling layer										
Kernel size	2	3	4	3	3	2	3	4	3	3
Stride	1	1	1	1	1	1	1	1	1	1
Global hyperparameters										
Learning rate	0.001	0.00075	0.0005	0.00075	0.00075	0.001	0.00075	0.0005	0.00075	0.00075

2.6. Evaluation metrics

To standardize the performance evaluation of the developed models, the root mean square error (RMSE) is employed as the primary metric to assess the generalization capability and predictive accuracy. Prior to model input, raw signals captured

by the sensory tool holder undergo FFT to transition from the time domain to the frequency domain. This transformation is critical for providing essential feature data to the input layers of the neural network, specifically the spectral magnitude of the cutting signals.

The RMSE is utilized to evaluate the accuracy of the regression models by calculating the square root of the average squared difference between the predicted values and the actual ground-truth values (dimensional accuracy or surface roughness). A lower RMSE value indicates that the model's predictions are closer to the experimental measurements, representing higher reliability. The mathematical expression for RMSE is defined:

$$RMSE=\sqrt{\frac{1}{n}\sum_{i=1}^{n}\left(y_i-\hat{y}_i\right)} \tag{3}$$

3. Results and Discussion

This chapter presents the experimental results and evaluates the predictive performance of the developed neural network models. The analysis begins with an examination of the acquired cutting force signals, dimensional accuracy, and surface roughness data collected during the SUS304 side milling experiments. Subsequently, the prediction results for both dimensional accuracy and surface roughness are reported and compared across the DNN, 1-D CNN, and 2-D CNN architectures. Statistical validation using the mann-whitney u test is also provided to assess model robustness. The following sections detail these findings and discuss their implications.

3.1. Analysis of machining signals and experimental data

The experimental phase generated a robust dataset comprising 1,326 cutting trials for SUS304 stainless steel, corresponding to 51 workpieces with 26 layers each. The primary objective of this section is to analyze the correlation between the acquired physical signals and the resulting machining quality, including dimensional accuracy, surface roughness, and tool wear progression.

3.1.1. Characteristics of cutting force signals

The Pro-micron sensory tool holder successfully captures high-fidelity signals across six channels, including tension, torsion, bending moments (XZ and YZ), time, and temperature. Among these, the bending moment in the XZ direction is identified as the most sensitive feature for predicting machining deviation. FFT analysis of the spindle under non-cutting conditions at 2,228 rpm exhibits a dominant peak at 37.5 Hz. This frequency corresponds to 2,250 rpm, confirming that the signal acquisition system accurately reflects the physical dynamics of the machining environment with minimal error.

3.1.2. Dimensional accuracy through in-process measurement

Dimensional data are systematically collected using the Renishaw OMP400 in-process measurement system. From the comprehensive dataset of 1,326 experimental trials, dimensional error values are recorded across successive layers. For the subsequent computational modeling, a subset of 100 trials is strategically sampled to train the neural network architectures. The in-process measurement system captures volumetric errors with a precision of 0.001 mm. The observed errors predominantly range between –0.13 mm and –0.4 mm. A notable outlier of –0.5 mm is detected at the 16th workpiece; this deviation is potentially attributable to material inhomogeneity or localized abnormal burr formation. These errors are primarily attributed to tool deflection and the pronounced work-hardening characteristics of SUS304, which establish a complex, non-linear mapping for the DNN and CNN models. The variation in dimensional errors during the machining process is illustrated in Fig. 7.

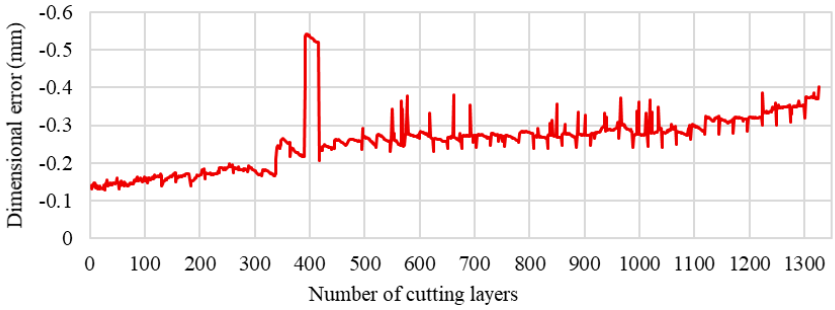

Fig. 7 Trend of dimensional error during the machining process

3.1.3. Surface roughness and tool wear progression

Surface quality is evaluated at 26-trial intervals, synchronized with the completion of each workpiece, resulting in a total of 51 data groups. For each group, topographical data from three distinct points on the machined surface are acquired using a 3D digital microscope (KEYENCE VHX-900F) and subsequently averaged to ensure representative results. Analysis of these results prioritizes Sa (arithmetical mean height) and Ra (arithmetical mean roughness) as key performance indicators. The recorded Sa values range from 1.1833 to 3.7407 μm, while Ra values vary between 1.0169 and 3.7273 μm. Fig. 8 illustrates the evolution of surface roughness throughout the machining process.

Tool wear is monitored systematically throughout the experimental trials, with visual inspections revealing a pattern of progressive degradation. The initial cutting edge chips at the 208th layer, followed by subsequent failures of the second, third, and fourth edges at the 364th, 806th, and 1,092nd layers, respectively. These observations provide critical timestamps for correlating cutting signal variations with physical tool degradation. As tool wear advances, a clear upward trend in bending moment amplitude is observed. Interestingly, surface roughness values show a noticeable decline after approximately 400 cutting trials. This reduction is attributed to the damaged cutting edges acting as a form of rolling or burnishing on the machined surface, thereby altering the topography and lowering measured roughness despite increased tool wear. This phenomenon underscores the complex interplay between tool degradation and surface finish in prolonged machining operations.

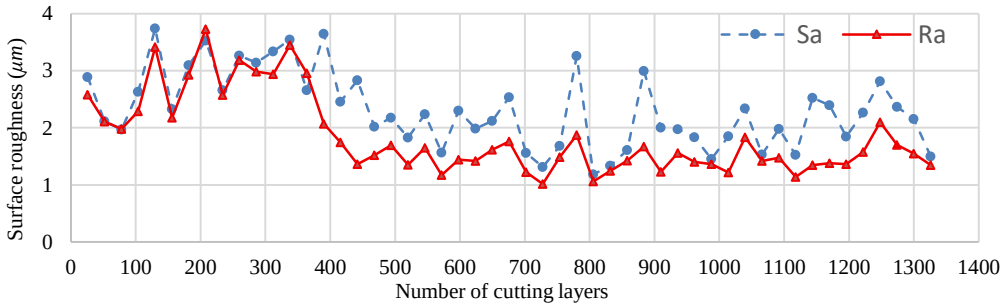

Fig. 8 Trend of surface roughness during the machining process

3.2. Results and discussion of predictive models

This study evaluated ten distinct parameter configurations for each neural network architecture to identify the optimal framework for predicting the machining quality of SUS304 stainless steel. The RMSE is utilized as the primary performance metric, where a lower value signifies superior generalization capability and higher predictive precision.

3.2.1. Analysis of dimensional accuracy prediction

All three neural network architectures achieve convergence during the prediction of dimensional accuracy. The training results are shown in Tables 7-9. Among the ten parameter configurations tested for each model, the DNN architecture demonstrates the highest precision and stability. The optimal DNN model (Parameter Group II) achieves an average RMSE of 0.0194 mm and a mean error percentage of 5.59%. In comparison, the best-performing 1-D CNN and 2-D CNN models yielded

higher RMSE values of 0.0212 mm and 0.0267 mm, respectively. The standard deviation of error percentages across all parameter groups is lowest for the DNN at 0.699%. In comparison, the 1-D CNN and 2-D CNN yield higher deviations of 1.93% and 1.56%, respectively. These results indicate that the fully connected DNN structure provided the most robust and accurate mapping between processed cutting force signals and dimensional errors for this specific task.

To provide a clearer comparison of model performance while avoiding visual clutter caused by overplotting, the prediction results are summarized using statistical error representations. Fig. 9 presents prediction error trends of different models for dimensional accuracy as mean error values with corresponding standard deviation ranges. The error bars indicate the variability of model performance across repeated experiments, enabling comparison of both prediction accuracy and stability.

Table 7 Training results of dimensional accuracy using the DNN model

Model	I	II	III	IV	V	VI	VII	VIII	IX	X	Standard deviation
RMSE results (unit: mm)											-
RMSE_1	0.0210	0.0196	0.0241	0.0228	0.0198	0.0248	0.0254	0.0277	0.0250	0.0230	-
RMSE_2	0.0161	0.0205	0.0260	0.0270	0.0219	0.0253	0.0256	0.0239	0.0231	0.0252	-
RMSE_3	0.0235	0.0181	0.0260	0.0260	0.0226	0.0252	0.0265	0.0279	0.0258	0.0258	-
Average	0.0202	0.0194	0.0254	0.0253	0.0214	0.0251	0.0258	0.0265	0.0246	0.0247	0.0025
Error results (unit: %)											-
Error_1	6.7645	5.6262	7.4306	6.7924	5.3224	6.9838	7.2898	8.0395	7.4534	7.7983	-
Error_2	5.5801	5.1447	8.1213	7.5247	7.1363	7.1822	7.4379	6.5687	7.4795	7.4247	-
Error_3	6.4361	5.9903	7.2221	7.6416	6.8958	6.9758	7.3998	7.5875	7.8430	7.7988	-
Average	6.2602	5.5871	7.5913	7.3196	6.4515	7.0472	7.3758	7.3986	7.5919	7.6739	0.699

Table 8 Training results of dimensional accuracy using the 1-D CNN model

Model	I	II	III	IV	V	VI	VII	VIII	IX	X	Standard deviation
RMSE results (unit: mm)											-
RMSE_1	0.0181	0.0489	0.0214	0.0324	0.0400	0.0370	0.0274	0.0337	0.0224	0.0364	-
RMSE_2	0.0239	0.0395	0.0411	0.0427	0.0422	0.0396	0.0368	0.0205	0.0315	0.0446	-
RMSE_3	0.0215	0.0338	0.0424	0.0428	0.0381	0.0438	0.0336	0.0334	0.0398	0.0381	-
Average	0.0212	0.0407	0.0349	0.0393	0.0401	0.0401	0.0326	0.0292	0.0312	0.0397	0.0064
Error results (unit: %)											-
Error_1	6.9825	12.8697	6.0833	9.2193	12.3308	12.8239	9.7948	11.7684	8.5230	12.6892	-
Error_2	9.0230	12.9768	11.6886	12.3576	13.5105	11.7947	12.1477	6.5500	9.8671	13.0837	-
Error_3	5.3200	10.2476	12.0870	14.3574	13.4724	15.2085	9.2032	10.8269	9.3650	9.9265	-
Average	7.1085	12.0314	9.9530	11.9781	13.1046	13.2757	10.3819	9.7151	9.2517	11.8998	1.932

Table 9 Training results of dimensional accuracy using the 2-D CNN model

Model	I	II	III	IV	V	VI	VII	VIII	IX	X	Standard deviation
RMSE results (unit: mm)											-
RMSE_1	0.0154	0.0332	0.0362	0.0290	0.0330	0.0255	0.0322	0.0324	0.0210	0.0275	-
RMSE_2	0.0260	0.0353	0.0385	0.0297	0.0265	0.0220	0.0401	0.0354	0.0565	0.0333	-
RMSE_3	0.0284	0.0307	0.0349	0.0213	0.0377	0.0278	0.0302	0.0181	0.0186	0.0391	-
Average	0.0233	0.0331	0.0365	0.0267	0.0324	0.0251	0.0342	0.0286	0.0320	0.0333	0.0043
Error results (unit: %)											-
Error_1	5.3413	10.4736	11.3560	7.6958	8.7649	9.1769	10.9040	10.7103	6.0866	10.1750	-
Error_2	8.3796	10.1486	12.6648	9.0172	10.1660	7.0050	11.3894	8.6885	14.5609	11.1761	-
Error_3	9.4769	10.5607	10.8831	6.4282	12.4795	8.8067	11.1385	5.2700	6.3807	12.7899	-
Average	7.7326	10.3943	11.6346	7.7137	10.4701	8.3295	11.1440	8.2229	9.0094	11.3803	1.563

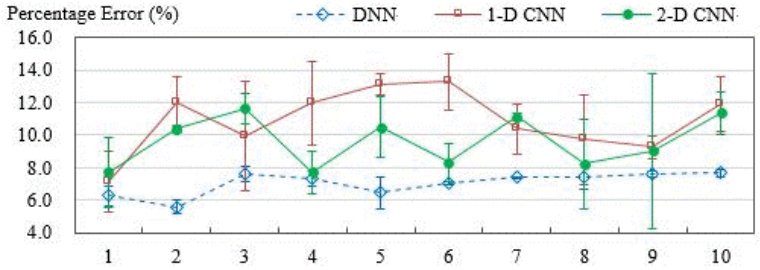

Fig. 9 Prediction error trends of different models for dimensional accuracy

3.2.2. Analysis of surface roughness prediction

For the prediction of surface roughness, the DNN architecture again showed superior consistency. Its optimal configuration (Parameter Group VIII) results in an RMSE of 0.3950 μm with a mean error of 12.63%. The best 1-D CNN model, specifically Parameter Group III, achieves a slightly lower RMSE of 0.2489 μm. However, its performance across different parameter sets is less stable than the DNN. This is evidenced by a higher standard deviation of error percentages, which reaches 3.31% for the 1-D CNN compared to only 1.04% for the DNN.

In contrast, the 2-D CNN model exhibits the greatest variability and higher average prediction errors among the three architectures, with an error standard deviation of 2.17%. These results suggest that, despite the slightly lower minimum RMSE achieved by the 1-D CNN, the DNN model provides a more reliable and consistent prediction performance overall. Therefore, for surface roughness prediction under the present experimental conditions, the DNN architecture is considered the most suitable model due to its balanced performance in terms of accuracy and robustness. The training results are shown in Tables 10-12.

Table 10 Training results of surface roughness using the DNN model

Model	I	II	III	IV	V	VI	VII	VIII	IX	X	Standard deviation
RMSE results (unit: μm)											-
RMSE_1	0.4647	0.4717	0.4641	0.4466	0.4941	0.4241	0.5153	0.3780	0.4689	0.3051	-
RMSE_2	0.4784	0.4800	0.5213	0.5342	0.4454	0.4806	0.4616	0.4144	0.4255	0.4736	-
RMSE_3	0.5031	0.4653	0.4797	0.4290	0.4603	0.3860	0.4140	0.3927	0.3795	0.3907	-
Average	0.4821	0.4723	0.4884	0.4699	0.4666	0.4302	0.4636	0.3950	0.4246	0.3898	0.036
Error results (unit: %)											-
Error_1	12.7939	16.1695	15.1852	16.0335	13.9964	12.7110	14.4343	12.1779	15.1378	13.6626	-
Error_2	13.0292	15.4449	15.6916	16.0124	15.0601	14.8528	14.0652	12.8990	15.4384	13.7492	-
Error_3	14.0705	14.7930	14.5190	15.1515	14.8235	12.8620	12.5994	12.8048	13.9042	13.3183	-
Average	13.2979	15.4691	15.1319	15.7325	14.6267	13.4753	13.6996	12.6272	14.8268	13.5767	1.04

Table 11 Training results of surface roughness using the 1-D CNN model

Model	I	II	III	IV	V	VI	VII	VIII	IX	X	Standard deviation
RMSE results (unit: μm)											-
RMSE_1	0.4232	0.3060	0.2528	0.2808	0.3851	0.4527	0.3334	0.5113	0.5727	0.4067	-
RMSE_2	0.5628	0.3628	0.2500	0.2395	0.2926	0.4745	0.2973	0.5197	0.4812	0.4183	-
RMSE_3	0.3267	0.3163	0.2440	0.2979	0.2718	0.4626	0.3141	0.5174	0.5333	0.2934	-
Average	0.4376	0.3284	0.2489	0.2728	0.3165	0.4633	0.3150	0.5161	0.5291	0.3728	0.10
Error results (unit: %)											-
Error_1	14.5172	13.3087	12.6491	13.3518	14.3892	18.6119	14.8001	17.1528	20.4877	17.9778	-
Error_2	16.1395	15.7478	10.7380	12.1472	14.5357	20.3508	11.7916	21.4985	20.6179	19.4499	-
Error_3	10.8431	13.5904	9.9618	11.4484	10.5637	16.2453	13.3797	18.9260	22.2048	12.7763	-
Average	13.8333	14.2156	11.1163	12.3158	13.1629	18.4027	13.3238	19.1925	21.1035	16.7347	3.31

Table 12 Training results of surface roughness using the 2-D CNN model

Model	I	II	III	IV	V	VI	VII	VIII	IX	X	Standard deviation
RMSE results (unit: μm)											
RMSE_1	0.3715	0.5847	0.5253	0.3832	0.5843	0.4723	0.4034	0.4440	0.3770	0.3325	-
RMSE_2	0.3498	0.3174	0.5203	0.5462	0.5146	0.3258	0.5295	0.4152	0.4043	0.2786	-
RMSE_3	0.5077	0.5203	0.3502	0.6136	0.6622	0.2241	0.4048	0.4089	0.4686	0.5023	-
Average	0.4097	0.4741	0.4653	0.5143	0.5870	0.3407	0.4459	0.4227	0.4166	0.3711	0.07
Error results (unit: %)											-
Error_1	14.0835	22.5959	16.9726	19.4280	20.7593	18.0077	19.3639	19.6776	18.9335	14.6264	-
Error_2	17.1406	12.1239	16.9882	19.0121	21.7673	12.2065	17.1574	15.5756	16.6284	13.5044	-
Error_3	18.9809	20.5045	13.5413	21.2671	20.8289	11.5831	17.3736	19.4042	16.7250	16.9831	-
Average	16.7350	18.4081	15.8340	19.9024	21.1185	13.9324	17.9650	18.2191	17.4290	15.0380	2.17

Fig. 10 presents prediction error trends of different models for surface roughness as mean error values with corresponding standard deviation ranges. This representation highlights the comparative performance and robustness of each model, particularly under limited data availability.

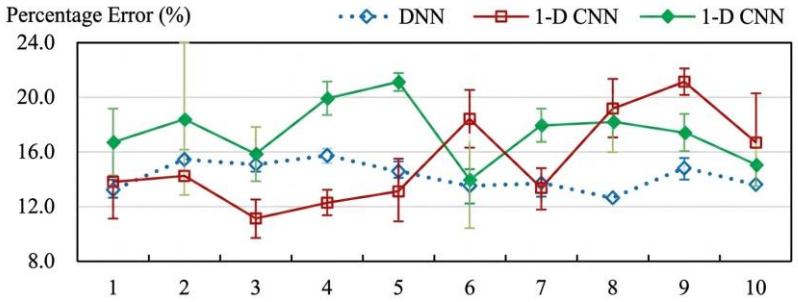

Fig. 10 Prediction error trends of different models for surface roughness

3.2.3. Training dynamics and convergence analysis

To assess the risk of overfitting, the training and validation loss curves are monitored for all models. Fig. 11 shows the loss curves of the 2-D CNN model during dimensionality accuracy prediction; a similar trend is observed for surface roughness prediction. The training loss steadily decreases and stabilizes after approximately 80 epochs, while the validation loss shows a similar trend without significant increase, indicating good generalization ability and no overfitting. The final validation loss reaches a plateau with low variance, confirming the model's convergence. Training is terminated early when the validation loss does not improve for 100 consecutive epochs. The gap between the training and validation losses remains small (root mean square error less than 0.002), further confirming that the model is not overfitting. The same trend is observed for the DNN and 1-D CNN models, although the final loss value for the DNN is smaller.

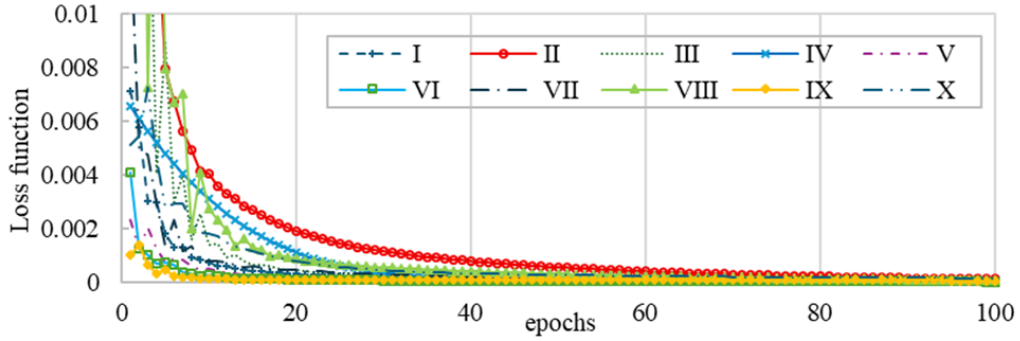

Fig. 11 Training and validation loss curves for the 2-D CNN model (dimensional accuracy prediction)

3.3. Comprehensive discussion and model comparison

By synthesizing the experimental data and predictive outcomes, this study draws the following conclusions:

(1) Optimal Architecture for the Task: although CNNs are typically advantageous for capturing spatial or sequential patterns, the DNN demonstrates superior performance and greater robustness in predicting the dimensional accuracy and surface roughness of the SUS304 machining dataset. The reliability of the DNN is evidenced by its consistently lower standard deviation of prediction errors, specifically 0.70% for dimensional accuracy and 1.04% for surface roughness across multiple parameter configurations. This architecture effectively outperforms both 1-D and 2-D CNN variants in terms of predictive stability.

(2) Feature Processing Insight: the success of the DNN suggests that the pre-processed cutting force features, such as those derived from FFT analysis, provide a sufficiently informative representation of the machining process. Consequently, the fully connected layers effectively learn the complex, non-linear relationships between these features and the macroscopic machining outcomes. This performance indicates that the localized feature extraction of CNNs is unnecessary for achieving high predictive accuracy in this application.

(3) Model Selection Guidance: for in-process quality prediction systems in similar machining contexts where signal features are carefully engineered in the frequency domain, a well-tuned DNN can be a simpler and more reliable choice than more complex convolutional architectures; it offers stable performance with lower computational overhead and model variability.

3.4. Comparative analysis and limitations of CNN architectures

While CNNs are renowned for their proficiency in extracting local patterns from structured data, both the 1-D and 2-D CNN architectures underperform compared to the DNN in this study's predictive tasks. While 1-D CNNs are theoretically adept at identifying localized spectral signatures, such as resonant peaks associated with tool wear, their performance remained inferior compared to the DNN in the current study. The DNN demonstrates superior stability, evidenced by a standard deviation in prediction error for dimensional accuracy of only 0.70%, which is significantly lower than the 1.93% recorded for the 1-D CNN.

This finding suggests that the critical signal variations stemming from the work hardening of SUS304 and progressive tool wear manifest as gradual shifts in the global energy distribution across the frequency spectrum, rather than as isolated local features. Consequently, the fully connected layers of the DNN prove more robust in modeling these global nonlinear relationships than the localized filters of the 1-D CNN.

The input for the 2-D CNN is constructed by reshaping the 1-D spectral sequence into a 2-D matrix, a transformation intended to leverage 2-D kernels for capturing spatial patterns within a pseudo-image. Despite its greater theoretical capacity, the 2-D CNN yields the lowest predictive accuracy among the three architectures. The primary limitation is that this reshaping process lacks a physical or causal foundation; it arbitrarily disrupts the native adjacency relationships and structural integrity of the frequency components. Hence, the spatial correlations targeted by the 2-D convolutional filters are nonexistent in the actual data, leading to the extraction of spurious features and poor model generalization.

3.5. Statistical validation of model robustness

To substantiate the claim that the DNN exhibits superior robustness over CNN architectures, a Mann-Whitney U test is performed to compare the prediction error distributions across ten independent parameter configurations for each model. This non-parametric approach ensures statistical validity without assuming a normal distribution for the RMSE values. The results are summarized in Table 13, with key findings highlighted as follows:

(1) Dimensional Accuracy: the DNN significantly outperforms both the 1-D CNN ($U = 0$, $p = 0.002$) and the 2-D CNN ($U = 0$, $p = 0.002$).

(2) Surface Roughness: the DNN again demonstrates significantly lower errors compared to the 1-D CNN ($U = 2$, $p = 0.004$) and the 2-D CNN ($U = 0$, $p = 0.002$).

These results reject the null hypothesis, statistically confirming that the lower mean errors and reduced variability observed in the DNN are unlikely to have occurred by chance. Consequently, the robustness claim for the DNN is empirically supported beyond descriptive statistics. The extremely low U values and significant p-values indicate a consistent and substantial performance advantage of the DNN's fully connected architecture over the convolutional models in this specific frequency-domain prediction task.

Table 13 Statistical comparison of prediction errors between DNN and CNN architectures

Target	Model comparison	Mean error (%)	Std (%)	Mann-whitney u	P-value	Effect size (r)
Dimensional accuracy	DNN vs. 1-D CNN	5.59 vs. 12.03	0.70 vs. 1.93	0	0.002	0.98
Dimensional accuracy	DNN vs. 2-D CNN	5.59 vs. 7.71	0.70 vs. 1.56	0	0.002	0.98
Surface roughness	DNN vs. 1-D CNN	12.63 vs. 19.19	1.04 vs. 3.31	2	0.004	0.96
Surface roughness	DNN vs. 2-D CNN	12.63 vs. 18.22	1.04 vs. 2.17	0	0.002	0.98

4. Conclusions

This study developed neural network models for in-process quality prediction in SUS304 milling. A sensory toolholder was integrated with an automated measurement system to acquire high-fidelity cutting force signals. These signals were processed into frequency-domain features to evaluate DNN and CNN architectures. Based on the findings, the following conclusions are drawn:

(1) System integration: the pro-micron sensory tool holder and Renishaw OMP400 system enabled real-time data acquisition. This integration successfully reduced manual inspection downtime.

(2) Model superiority: the DNN was the most robust model, balancing accuracy and stability. This success shows that FFT-based features allow fully connected layers to learn global nonlinear relationships effectively.

(3) Architectural performance: convolutional models underperformed compared to DNN. The 1-D CNN's variability suggests that quality indicators manifest as broad spectral shifts rather than local features. The 2-D CNN performed worst because reshaping 1-D spectral data into a 2-D matrix misaligned with the model's spatial inductive bias.

(4) Practical implications: effective implementation in smart manufacturing requires aligning network architecture with signal physics. For frequency-domain features, a well-tuned DNN is more reliable and efficient than complex convolutional models for adaptive control.

(5) Industrial deployment Paths: to transition this framework from a laboratory setting to a production environment, future work will focus on edge computing integration. By deploying the trained DNN onto edge devices local to the CNC machine tool, the system can achieve ultra-low latency inference, enabling real-time adaptive control of cutting parameters to mitigate quality deviations.

(6) Scalability and sustainability: this holistic framework offers a scalable solution for machining other difficult-to-cut materials. Implementing such intelligent monitoring systems can contribute to sustainable manufacturing by reducing scrap rates and optimizing tool life through data-driven decision-making.

Conflicts of Interest

The authors declare no conflict of interest.

References

[1] W. T. Chien and C. Y. Chou, "The Predictive Model for Machinability of 304 Stainless Steel," Journal of Materials Processing Technology, vol. 118, no. 1-3, pp. 442-447, 2001.

[2] M. H. Tsai, J. N. Lee, H. D. Tsai, M. J. Shie, T. L. Hsu, and H. S. Chen, "Applying a Neural Network to Predict Surface Roughness and Machining Accuracy in the Milling of SUS304," Electronics, vol. 12, no. 4, article no. 981, 2023.

[3] C. Wang, Y. Li, F. Gao, K. Wu, K. Yin, P. He, et al., "Milling-Force Prediction Model for 304 Stainless Steel Considering Tool Wear," Machines, vol. 13, no. 1, article no. 72, 2025.

[4] A. Schuster, A. Otto, H. Rentzsch, and S. Ihlenfeldt, "Multi-Sensory Tool Holder for Process Force Monitoring and Chatter Detection in Milling," Sensors, vol. 24, no. 17, article no. 5542, 2024.

[5] T. Souflas, E. Triantopoulou, C. Papaioannou, C. Ramsauer, J. A. Greitler, P. Schörghofer, et al., "Tool Condition Monitoring in Milling Using Cutting Force and Temperature Data from an Instrumented Milling Head," The International Journal of Advanced Manufacturing Technology, vol. 139, pp. 6049-6072, 2025.

[6] G. K. Ojha, G. K. Yadav, and P. K. Yadav, "Optimization Technique for Surface Roughness Prediction in Turning Operation," SAMRIDDHI A Journal of Physical Sciences, Engineering and Technology, vol. 6, no. 2, pp. 117-124, 2015.

[7] P. B. Huang, "An Intelligent Neural-Fuzzy Model for an In-Process Surface Roughness Monitoring System in End Milling Operations," Journal of Intelligent Manufacturing, vol. 27, no. 3, pp. 689-700, 2016.

[8] Z. Lu, M. Wang, and W. Dai, "Machined Surface Quality Monitoring Using a Wireless Sensory Tool Holder in the Machining Process," Sensors, vol. 19, no. 8, article no. 1847, 2019.

[9] Y. W. Chen, Y. F. Huang, K. T. Wu, and H. H. Lee, "Cutting Force Validation and Volumetric Errors Compensation of Thin Workpieces with Sensory Tool Holder," The International Journal of Advanced Manufacturing Technology, vol. 108, no. 1-2, pp. 299-312, 2020.

[10] L. Nowakowski, M. Bartoszuk, M. Skrzyniarz, S. Blasiak, and D. Vasileva, "Influence of the Milling Conditions of Aluminium Alloy 2017A on the Surface Roughness," Materials, vol. 15, no. 10, article no. 3626, 2022.

[11] M. H. Tsai, J. N. Lee, M. J. Shie, and M. H. Deng, "Intelligent Performance Prediction of Flank Milling of Ti6Al4V Using Sensory Tool Holder," Sensors and Materials, vol. 34, no. 8, pp. 3241-3253, 2022.

[12] P. Krishnakumar, K. Rameshkumar, and K. I. Ramachandran, "Tool Wear Condition Prediction Using Vibration Signals in High Speed Machining (HSM) of Titanium (Ti-6Al-4V) Alloy," Procedia Computer Science, vol. 50, pp. 270-275, 2015.

[13] Z. Huang, J. Zhu, J. Lei, X. Li, and F. Tian, "Tool Wear Predicting Based on Multi-Domain Feature Fusion by Deep Convolutional Neural Network in Milling Operations," Journal of Intelligent Manufacturing, vol. 31, no. 4, pp. 953-966, 2020.

[14] T. Pan, J. Zhang, X. Zhang, W. Zhao, H. Zhang, and B. Lu, "Milling Force Coefficients-Based Tool Wear Monitoring for Variable Parameter Milling," The International Journal of Advanced Manufacturing Technology, vol. 120, pp. 4565-4580, 2022.

[15] Y. W. Chan, T. C. Kang, C. T. Yang, C. H. Chang, S. M. Huang, and Y. T. Tsai, "Tool Wear Prediction Using Convolutional Bidirectional LSTM Networks," The Journal of Supercomputing, vol. 78, no. 1, pp. 810-832, 2022.

[16] F. C. Zegarra, J. Vargas-Machuca, and A. M. Coronado, "A Comparative Study of CNN, LSTM, BILSTM, and GRU Architectures for Tool Wear Prediction in Milling Processes," Journal of Machine Engineering, vol. 23, no. 4, pp. 122-136, 2023.

[17] J. Kurek, E. Świderska, and K. Szymanowski, "Tool Wear Classification in Chipboard Milling Processes Using 1-D CNN and LSTM Based on Sequential Features," Applied Sciences, vol. 14, no. 11, article no. 4730, 2024.

[18] M. Huang, X. Xie, W. Sun, and Y. Li, "Tool Wear Prediction Model Using Multi-Channel 1D Convolutional Neural Network and Temporal Convolutional Network," Lubricants, vol. 12, no. 2, article no. 36, 2024.

[19] I. Zagórski, M. Kulisz, and A. Semeniuk, "Artificial Neural Network Modelling of Cutting Force Components in Milling," ITM Web of Conferences, vol. 15, article no. 02001, 2017.

[20] S. Gao, X. Duan, K. Zhu, and Y. Zhang, "Generic Cutting Force Modeling with Comprehensively Considering Tool Edge Radius, Tool Flank Wear and Tool Runout in Micro-End Milling," Micromachines, vol. 13, no. 11, article no. 1805, 2022.